

Relativistic Distortions in the X-ray Spectrum of Cyg X-1

C. Done¹, P.T. Źycki^{1,2}

¹ Department of Physics, University of Durham, South Road, Durham, DH1 3LE

² Nicolaus Copernicus Astronomical Center, Bartycka 18, 00-716 Warsaw

8 March 2018

ABSTRACT

We present the first significant detection of relativistic smearing of the X-ray reflection spectrum from the putative accretion disk in the low/hard state of Cyg X-1. The ionization state, and amount of relativistic smearing are simultaneously constrained by the X-ray spectra, and we conclude that the disk is not strongly ionized, does not generally extend down to the last stable orbit at 3 Schwarzschild radii and covers rather less than half the sky as seen from the X-ray source. These results are consistent with a geometry where the optically thick disk truncates at a few tens of Schwarzschild radii, with the inner region occupied by the X-ray hot, optically thin(ish) plasma. Such a geometry is also inferred from previous studies of the reflected spectrum in Galactic Black Hole transient sources, and from detailed considerations of the overall continuum spectral shape, suggesting that this is a robust feature of low/hard state accretion onto Galactic Black Holes.

Key words: accretion, accretion discs – binaries: close – black hole physics – stars: individual (Cygnus X-1) – X-ray: general – X-ray: stars

1 INTRODUCTION

Some of the strongest evidence for the existence of black holes has come from recent ASCA (0.6–10 keV) X-ray observations of the shape of the iron K α line in Active Galactic Nuclei (AGN). AGN typically produce copious hard X-ray emission, and the iron line is formed from fluorescence as these X-rays illuminate the infalling material. The combination of Doppler effects from the high orbital velocities and strong gravity in the vicinity of a black hole gives the line a characteristically skewed, broad profile (Fabian et al., 1989). This has been unambiguously identified from ASCA 0.6–10 keV spectra of the AGN MCG-6-30-15, where the breadth of the line profile implies that the accretion disk extends down to *at least* $6R_g$, the last stable orbit in a Schwarzschild metric (Tanaka et al 1995; Iwasawa et al 1996).

As well as producing the line, some fraction of the illuminating hard X-rays are reflected from the accretion flow, producing a characteristic continuum spectrum. The amplitude of the line and reflected continuum depend on the amount of material being illuminated by the hard X-rays, its inclination, elemental abundances and ionization state (e.g. Lightman & White 1988; George & Fabian 1991; Matt, Perola & Piro 1991; Ross & Fabian 1993; Źycki & Czerny 1994). The mean amount of reflection and line seen in Seyfert 1 AGN is consistent with a power law X-ray spectrum illuminating an optically thick, (nearly) neutral disk, which subtends a solid angle of $\sim 2\pi$ (Pounds et al 1990; Nandra

& Pounds 1994), although it is now recognised that individual objects show significant dispersion about this mean (Zdziarski, Lubiński & Smith 1999).

This contrasts with the situation in the Galactic Black Hole Candidates (GBHC). These are also thought to be powered by accretion via a disk onto a black hole, and, in their low/hard state, show spectra which are rather similar to those from AGN. However, the amount of reflection and iron line is much less than would be expected from an accretion disk which subtends a solid angle of 2π (e.g. Gierliński et al 1997a), and the detected line is narrow, with no obvious broad component (Marshall et al 1993, Ebisawa et al 1996, hereafter E96). There are (at least) two possible explanations for this: firstly that it is an artifact of the difference in ionization state of the disk between GBHC and AGN, or secondly that there is a real difference in geometry between the supermassive accreting black holes and the stellar mass ones.

Ionization differences seems at first sight to be an extremely attractive option. For accretion at the same fraction of Eddington, the disk temperature should scale as $M^{-1/4}$. The GBHC inner disk is then expected to be a factor of ~ 30 hotter than in AGN, and the higher expected ionization state from the thermal ion populations gives a reflected continuum and associated iron line that can be very different to that from a neutral disk (Lightman & White 1988; Ross & Fabian 1993; Matt Fabian & Ross 1993ab; Źycki et al 1994; Matt Fabian & Ross 1996; Ross, Fabian & Brandt

1996). As well as increasing the energy of the iron edge (and line), ionization also reduces the low energy opacity of the disk, and so enhances its reflectivity. However, the iron edge (whatever its energy) has a fairly constant cross-section, so the net result is to increase the relative strength of the iron edge feature in the reflected continuum. There is also the possibility of the line being suppressed through resonant absorption over a (rather small) range in ionization states, so the net result can be a prominent edge without obvious line emission accompanying it. Such models were proposed as the solution to the weak line emission seen in GBHC compared to AGN (Ross & Fabian 1993; Matt et al., 1993a; Ross et al 1996).

However, detailed spectral fitting with photo-ionized reflected continua shows that the ionization state of the reflector is in general too low for the resonant absorption process to be important. This argues against such models, although relativistic shifts could affect the derived ionization states (Matt et al 1993a, Ross et al., 1996). Another way to suppress both line and reflected continuum is from a radial dependance of ionization state. If the inner region of the disk were so highly ionized that they produce no atomic features then their contribution to the reflected continuum is unobservable in the 2–20 keV range. Here we fit data from Cyg X-1 with a reflection model which includes both ionization (as a function of radius) and relativistic smearing in order to test whether the spectra are indeed affected by resonant absorption and whether radial ionization structure is important in masking the reflection signature.

We significantly detect relativistic smearing of the reprocessed features in Cyg X-1, and find that the disk is not highly ionized. This apparently rules out both featureless (extreme ionization) reflection and resonant absorption. The line is not suppressed relative to the reflected continuum, it is merely broadened by the relativistic effects which made it difficult to detect in ASCA data (E96), where the observed weak and narrow line emission probably comes from the companion star. The derived covering fraction of the relativistic reflector is substantially less than expected from a flat disk. The most plausible explanation for this is that the optically thin(ish) X-ray corona fills a central ‘hole’, so that less than half of the X-ray flux intercepts the disk. The amount of relativistic smearing generally is inconsistent with the disk extending down to the last stable orbit at $6R_g$. These results from the shape of the reprocessed spectrum are remarkably similar to the geometry derived from energetic arguments from the continuum spectral shape (Gierliński et al. 1997a; Dove et al 1997; Poutanen, Krolik & Ryde 1997). Equally, they are very similar to the derived reflection geometry from spectra of transient GBHC during their decline (Źycki, Done & Smith 1997; Źycki, Done & Smith 1998ab), pointing to a single, fairly stable geometry for the low/hard state GBHC.

2 THE SPECTRAL MODEL

The reflection model is described in detail in Źycki et al (1998b). Basically it consists of the angle dependant reflection code of Magdziarz & Zdziarski (1995), with ion populations calculated as in Done et al (1992), as implemented in the ‘pexriv’ model in XSPEC. This determines the ion

populations by balancing photoelectric absorption against radiative recombination. The photo-electric absorption edge energies for iron were corrected from the rather approximate values given by Reilman & Manson (1978) to those of Kaasstra & Mewe (1994). As noted by E96, these give a significant difference in the derived ionization state. Photo-ionization rates are strongly dependent on the parameter $\xi = L/(nr^2)$ ergs s^{-1} cm^{-1} (where L is the ionizing luminosity, here taken to be between 5eV and 20 keV, n is the density and r the distance of the material from the ionizing flux) and weakly on spectral shape (assumed here to be a power law), while recombination depends on temperature (assumed fixed at 10^6 K). The self-consistent iron line is then calculated from the Monte-Carlo code of Źycki & Czerny (1994) and added to the continuum. We assume fixed ‘solar’ abundances from Morrison & McCammon (1983), except for iron, which is free to vary from its tabulated value of $Fe/H = 3.3 \times 10^{-5}$.

Ionization as a function of radius can easily be treated by adding together many radial rings with ionization $\xi(r) \propto r^\beta$, where the relative covering fraction for each ring can be calculated from the X-ray irradiation $F_{\text{irr}}(r) \propto r^{-3}$.

The relativistic smearing is taken from the XSPEC ‘diskline’ model, with slight modifications to take light bending into account (Fabian et al 1989). This is parameterised by the inner and outer radius of the disk, R_{in} and R_{out} , its inclination and (again) the irradiation emissivity, $F_{\text{irr}}(r) \propto r^{-3}$. We fix $R_{\text{out}} = 10^4 R_g$ (where $R_g = GM/c^2$) and fit for R_{in} , convolving the relativistic transfer function with the total (line plus continuum) reprocessed spectrum. For the multiple ionization state disk the relativistic transfer function is calculated for each annulus, convolved with the reprocessed spectrum from that ring and then co-added to get the total spectrum.

We assume a power law illuminating spectrum. This is an approximation to the true shape of a Comptonised spectrum and it becomes a poor description at energies close to the seed photon energy and close to the electron temperature. Typically in low/hard state of Cyg X-1 the electron temperature is ~ 100 keV (e.g. Gierliński et al 1997a), so this will not give significant distortions to the spectral range considered here, which is always ≤ 20 keV.

The situation with regards the soft photons is less clearcut. The strongest component of the soft X-ray continuum can be modelled as a blackbody or disk blackbody with a temperature of $0.1 - 0.2$ keV (e.g. Balucińska & Hasinger 1991; E96; di Salvo et al 1998). Again, this is far enough away from the energy range considered in this paper (≥ 2 keV) for the distortions of the true Compton scattered spectrum from a power law to be negligible. However, there is also a *second* soft component which extends to higher energies (E96, di Salvo et al 1998). E96 modelled this in the ASCA data using a softer power law below a break energy around 3 keV, but such a broken power law is rather unphysical. Perhaps a more realistic model is one where soft photons from the accretion disk (at ~ 0.1 keV) are Comptonised by a rather cool population of electrons with $kT \sim 1$ keV as well as by the hot electrons with $kT \sim 150$ keV. The disk photons at ~ 0.1 keV are energetically more important, so it seems probable that this component at ~ 1 keV does not contribute significantly to the seed photons.

The physical origin of the second soft excess is entirely unknown, and so is its geometry with respect to the disk and

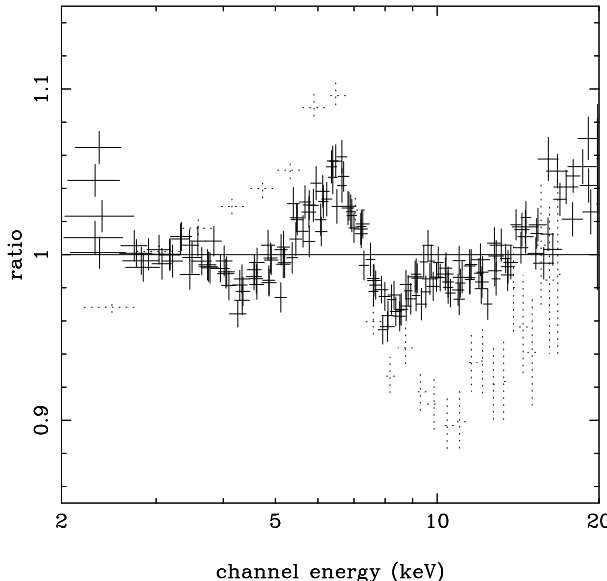


Figure 1. The ratio of each EXOSAT GSPC spectra of Cyg X-1 to a best fitting power law model. Both excess counts at the line energy and a deficit at the edge are seen, as in AGN. The dotted line shows the same ratio for the GINGA-12 AGN spectrum (Pounds et al 1990) for comparison.

hot plasma. It may or may not then produce its own reflected component. We assume it does not, but note that even if it does then its contribution to the crucial iron line and edge region will be very small due to the low temperature of this component.

In the following fitting we generally neglect data below 4 keV so as to avoid the complexities of the soft excess, and fix the galactic column at $6 \times 10^{21} \text{ cm}^{-2}$.

3 CONSTANT IONIZATION REFLECTION

3.1 EXOSAT GSPC data

The EXOSAT GSPC data from Cyg X-1 give some of the best spectra to date from this object, with the broad 2–20 keV energy range of GINGA data but resolution comparable to that of the ASCA GIS. We use the 5 GSPC spectra of Done et al., (1992). The residuals to the best fit simple power law for each GSPC spectrum are shown in Figure 1, together with the residuals to a simple power law fit to the GINGA-12 AGN spectrum of Pounds et al (1990). Contrary to claims by Ross et al (1996), Cyg X-1 is not dominated by the edge structure, but also shows a strong excess at the iron line energy. Also, *both* line and edge appear equally diminished in Cyg X-1 compared to AGN, although it is somewhat misleading to compare these residuals directly since Cyg X-1 is strongly absorbed by the interstellar medium and can have a substantial contribution at 2 keV from the observed soft excess.

We fit the 5 GSPC spectra simultaneously in XSPEC, although only the reflection parameters of inclination and iron abundance are constrained to be equal across all the datasets.

We first fit the 4–20 keV data with a power law. This gives a poor fit ($\chi^2_\nu = 1309/625$) due to the presence of

spectral features from iron (see Figure 1). Including a neutral reprocessed component inclined at 30° (Gies & Bolton 1986) gives a dramatic decrease in χ^2_ν to $677/620$, with a further significant improvement in the fit if this is allowed to be ionized ($\chi^2_\nu = 611/615$). Allowing the iron abundance to be a free parameter makes no significant difference, with $\chi^2_\nu = 610/614$ for $A_{\text{Fe}} = 0.9 \pm 0.2 \times \text{solar}$.

Allowing the reprocessed spectrum to be relativistically smeared gives a significantly better fit, with $\chi^2_\nu = 535/609$. We obtain constraints on the inner radius of the disk in each spectrum, and these are somewhat larger than the $6R_g$ expected for a disk extending down to the last stable orbit, assuming an illumination which is $\propto r^{-3}$. The derived iron abundance is $A_{\text{Fe}} = 1.8^{+0.7}_{-0.4} \times \text{solar}$ i.e. supersolar abundances are preferred. This is consistent with the $\sim 2 \times$ solar abundance of iron (given as $\text{Fe/H} = 6 \pm 1 \times 10^{-5}$) inferred for the stellar wind of the companion star from the strong edge feature seen in the absorbed ‘dip’ spectra (Kitamoto et al., 1984). The relativistic smearing allows more iron line to be present, since it is broad rather than narrow, so it is much less observable.

One potential problem may arise if there is a substantial narrow line component from X-ray illumination of flared outer regions of the disk and/or the companion star (Basko 1978) and stellar wind. This could distort the relativistic line fit, by adding a sharp core to the line profile. Such a line is indeed detected in high resolution BBXRT and ASCA data (Marshall et al 1993; E96). We allow for this by including a narrow Gaussian line at 6.4 keV, whose normalisation is a free parameter for each spectrum. This narrow component is not significantly detected in the GSPC data, since it reduces χ^2 by only ~ 1 for 5 additional parameters. The upper limits on the derived line equivalent widths are typically less than $\sim 30 \text{ eV}$, easily compatible with the ASCA and BBXRT detections. Clearly there should also be a reflection continuum accompanying this line unless a substantial portion of it arises from an optically thin stellar wind. We model this by including an additional, unsmeared, neutral reprocessed spectrum, assuming a fixed inclination of 60° . Again, this does not improve the fit ($\chi^2_\nu = 535/604$), but we include it for completeness. Details of this fit are given in Table 1, where the iron abundance is frozen at its best fit value of $1.8 \times \text{solar}$ so that the error bars can be calculated for each spectrum separately.

Several points are immediately apparent from this series of models. Firstly, the line strength is perfectly consistent with solar, or even supersolar abundances. It is not anomalously weak compared to the reflected continuum as proposed by Ross et al (1996). The reflector is significantly ionized, but not to the strength that would be required for Auger ionization to operate ($\xi \sim 300 - 1000$ for a power law of $\Gamma = 1.7$ and temperature of 10^6 K). The derived ionization state assuming an inclination of 30° is typically that of Fe VIII-XII, incompatible with the Auger range of Fe XVII – XXIII. These ionization states are obtained despite allowing for the effects of relativistic smearing. There is no conspiracy, whereby the high Auger ionization is masked by Doppler smearing and gravitational redshifts (Ross et al 1996). Instead the line and reflection continuum are perfectly consistent with each other, and with being produced in a disk which is weakly ionized.

Table 1. EXOSAT GSPC, GINGA and ASCA data from Cyg X-1. Error bars are $\Delta\chi^2 = 2.7$, Galactic column is fixed at $6 \times 10^{21} \text{ cm}^{-2}$, inclination at 30° and iron abundance at $1.8 \times \text{solar}$

dataset	PL Γ	PL Norm	$\Omega/2\pi_{\text{rel}}$	ξ	$R_{\text{in}}(R_{\text{g}})$	$\Omega/2\pi_{\text{non-rel}}$	χ^2_{ν}
GSPC 08	$1.75^{+0.02}_{-0.01}$	1.60	$0.21^{+0.04}_{-0.05}$	17^{+40}_{-16}	17^{+14}_{-8}	$0^{+0.07}$	89.2/118
GSPC 09	1.56 ± 0.02	1.24	$0.19^{+0.04}_{-0.07}$	24^{+90}_{-20}	13^{+9}_{-7}	$0^{+0.10}$	92.9/98
GSPC 10	1.58 ± 0.02	1.16	$0.11^{+0.04}_{-0.06}$	30^{+40}_{-26}	1000^{+952}_{-952}	$0^{+0.12}$	69.3/104
GSPC 13	$1.75^{+0.03}_{-0.02}$	2.35	0.24 ± 0.05	31^{+60}_{-29}	8^{+12}_{-2}	$0^{+0.11}$	174.8/176
GSPC 14	1.71 ± 0.02	1.75	0.22 ± 0.04	46^{+20}_{-42}	6.0^{+6}_{-6}	$0^{+0.03}$	108.7/109
GINGA 91-1	$1.60^{+0.05}_{-0.07}$	1.61	$0.23^{+0.09}_{-0.11}$	60^{+640}_{-58}	10^{+8}_{-4}	$0.07^{+0.03a}_{-0.07}$	10.2/21
GINGA 91-2	$1.61^{+0.03}_{-0.08}$	1.85	$0.29^{+0.06}_{-0.17}$	28^{+800}_{-28}	$28^{+\infty}_{-22}$	$0^{+0.1a}_{-0.1}$	9.8/21
GIS 1	1.87 ± 0.02	1.79	$0.05^{+0.03}_{-0.01}$	2300^{+6000}_{-1600}	16^{+7}_{-5}	$0^{+0.03}$	107.8/79
GIS 3	$1.84^{+0.02}_{-0.01}$	1.80	$0.06^{+0.03}_{-0.02}$	$3 \pm 2.4 \times 10^4$	58^{+110}_{-31}	0.04 ± 0.04	92.0/79
GIS 4	1.71 ± 0.02	1.24	0.1 ± 0.03	50^{+100}_{-28}	90^{+120}_{-40}	$0^{+0.05}$	142.8/79
SIS 5	1.68 ± 0.03	1.22	$0.09^{+0.78}_{-0.04}$	$3^{+32}_{-2} \times 10^4$	23^{+38}_{-11}	$0.05^{+0.08}_{-0.04}$	51.8/70
GIS 6	1.68 ± 0.02	1.89	$0.02^{+0.09}_{-0.01}$	$6.70^{+193}_{-90} \times 10^3$	31^{+210}_{-25}	$0.13^{+0.06}_{-0.05}$	84.4/79
GIS 7	$1.44^{+0.03}_{-0.02}$	0.93	$0.05^{+0.08}_{-0.02}$	$8.4^{+42}_{-7.9} \times 10^3$	14^{+14}_{-6}	$0^{+0.03}$	54.3/79
GIS 8	1.66 ± 0.02	1.44	$0.06^{+0.06}_{-0.04}$	115^{+1600}_{-90}	37^{+40}_{-21}	0.05 ± 0.05	108.2/79
GIS 9	1.59 ± 0.02	1.43	$0.09^{+0.09}_{-0.08}$	0^{+40}_{-2}	8^{+36}_{-2}	$0.13^{+0.05}_{-0.06}$	68.1/79
GIS 10	$1.60^{+0.03}_{-0.01}$	1.62	$0.06^{+0.11}_{-0.04}$	110^{+2000}_{-102}	64^{+100}_{-30}	0.08 ± 0.06	95.8/79

^a Parameter restricted to the range 0-0.1 since it is not well constrained

3.2 GINGA data

The GINGA data give consistent results, though at much lower significance. There were 3 epochs in which Cyg X-1 was observed, the first of which (August 1987) was mispointed and the remaining two (in May 1990 and June 1991) being in an unusual mode designed to increase the spectral range out to high energies. In this mode the spectral resolution is reduced by about a factor 2 since the same number of channels cover twice the bandpass. The resolution is then more like 30 per cent at iron, rather than 17 per cent in the usual mode. This is a crucial difference, since the broadest features expected from the inner disk are of order 30 per cent if the disk extends down to the last stable orbit, so these data are unlikely to be able to constrain the amount of relativistic smearing. Ironically, the larger bandpass is not actually of use either, as data beyond 30 keV are limited by uncertainties in background subtraction.

We use datasets 1 and 2 (the unabsorbed spectra) from the June 1991 observations shown by Gierliński et al (1997a). These are fit in the 4–30 keV range with the same model as above. The poor resolution of the data means that the relativistic smearing is not significantly detected, so the relativistic and non-relativistic reflected spectra are degenerate. From the EXOSAT results and from theoretical expectations of the amount of reflection from the companion star (Basko 1978) we limit the solid angle $\Omega/2\pi_{\text{non-rel}} \leq 0.1$. With this constraint we obtain the results shown in Table 1. Again the data have a line which is easily consistent with the amount of reflection seen. The observed ionization parameter of the reflecting material is generally low (though poorly constrained) even when relativistic distortions are included.

3.3 ASCA data

The ASCA SIS and GIS data used here are those published by E96, except that we neglect the October 1993 SIS spectra (spectrum 2 in E96) where there may be a residual problem with the resolution (E96). Again we use only data above 4 keV so as to avoid the complexities of the soft X-ray excess, and so that the fits can be compared with the results of E96. These data clearly show a narrow line component as well as a complex edge structure which has been modelled by an ionized reflection (E96). However, their reflected continuum model did not include the self-consistent iron line emission nor relativistic smearing.

The SIS spectrum has the best energy resolution (November 1993, denoted spectrum 5 in E96) so we first examine the line profile in these data. We fit this with the self-consistent iron line and continuum reflection code, together with a power law continuum and galactic $N_H = 6 \times 10^{21}$, firstly assuming an inclination of 30° . Without relativistic effects the fit is much worse than that shown by E96, with $\chi^2_{\nu} = 98/71$, showing that the narrow line cannot be the corresponding fluorescence from the material giving rise to the observed reflection continuum, irrespective of the iron abundance (best fit value of unity) and ionization ($\xi \sim 5$). Including relativistic effects gives a much better fit, with $\chi^2_{\nu} = 56/70$, comparable with that of E96. Including a separate narrow line gives an even better fit, with line energy and equivalent width of 6.46 keV and 10 eV ($\chi^2_{\nu} = 48/68$). However, physically we expect a self-consistent reflected continuum to accompany this line. Replacing the line with the total reprocessed spectrum from neutral material where relativistic effects are not important gives an equally good fit with $\chi^2_{\nu} = 51/69$. This fit (shown in Figure 2) is very different to the one derived from the EXOSAT data. The ionization is so high ($\xi \sim 4 \times 10^4$) that the ‘edge’ feature seen in the data is actually modelled by the drop following the

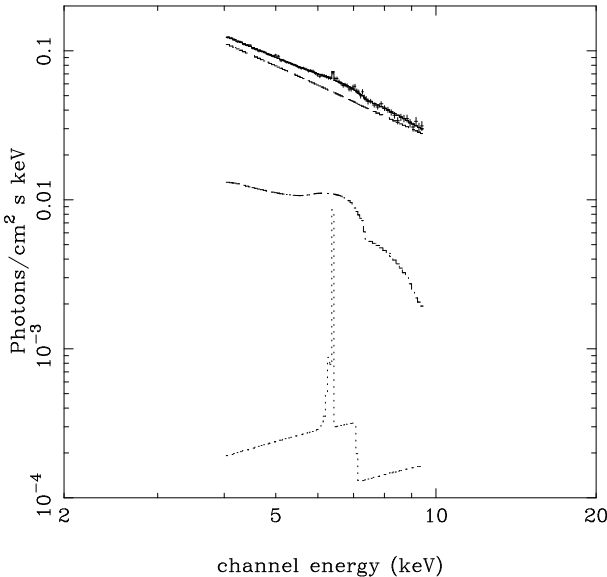


Figure 2. The best fit to the ASCA SIS 5 spectrum assuming an inclination of 30° , with iron abundance free to vary between $1 - 2 \times$ solar. The relativistic reflector has $\xi = 3.0^{+37}_{-2.2} \times 10^4$, $R_{\text{in}} = 23^{+40}_{-11}$ and $\Omega/2\pi = 0.09^{+0.81}_{-0.04}$, while the neutral unsmeared reflector has $\Omega/2\pi = 0.05^{+0.10}_{-0.04}$, for an illuminating power law with $\alpha = 0.68 \pm 0.03$ ($\chi^2_\nu = 51.8/70$).

relativistically smeared ($R_{\text{in}} \sim 22R_g$) ionized line, and the real edge is shifted outside of the observed energy range.

The GIS spectra give similar results. We fit these using the most recent GIS response matrices (as of March 1995, gis2v4-0.rmf) as opposed to the earlier response used by E96, and results are detailed in Table 1. Again, the derived ionization parameter is generally very high – only the GIS 4 and GIS 9 spectra give results that are anything like the low ionization EXOSAT and GINGA solutions.

3.4 Inclination

This general mismatch between the ionization of the reprocessor derived from ASCA and EXOSAT/GINGA data is suggestive of a systematic problem in the spectral model fitting, most likely due to the difference in bandpass. In EXOSAT and GINGA the high energy continuum shape of the reprocessed spectrum helps constrain its ionization, whereas in ASCA only the iron features can be used. The detailed shape of the line and edge is a strong function of inclination as well as of ionization. At high inclinations Doppler shifts prevail over gravitational and transverse redshift, shifting the line and edge to higher energies as well as giving substantial broadening. This is to zeroth order the same effect as ionization. However, the detailed shape of a low inclination, ionized reflection spectrum is rather different to a less ionized reflection spectrum at higher inclination, so these two parameters can be disentangled given good enough data.

Figure 3a shows how χ^2 varies for simultaneous spectral fitting of the five EXOSAT datasets as the disk inclination is changed from $30^\circ - 66^\circ$. Clearly there is a significant preference in the data for an inclination higher than 45° (cosine smaller than 0.7). The 3σ ($\Delta\chi^2 = 9$) limit to the inclination from this modelling is $i \geq 40^\circ$. This is rather higher than

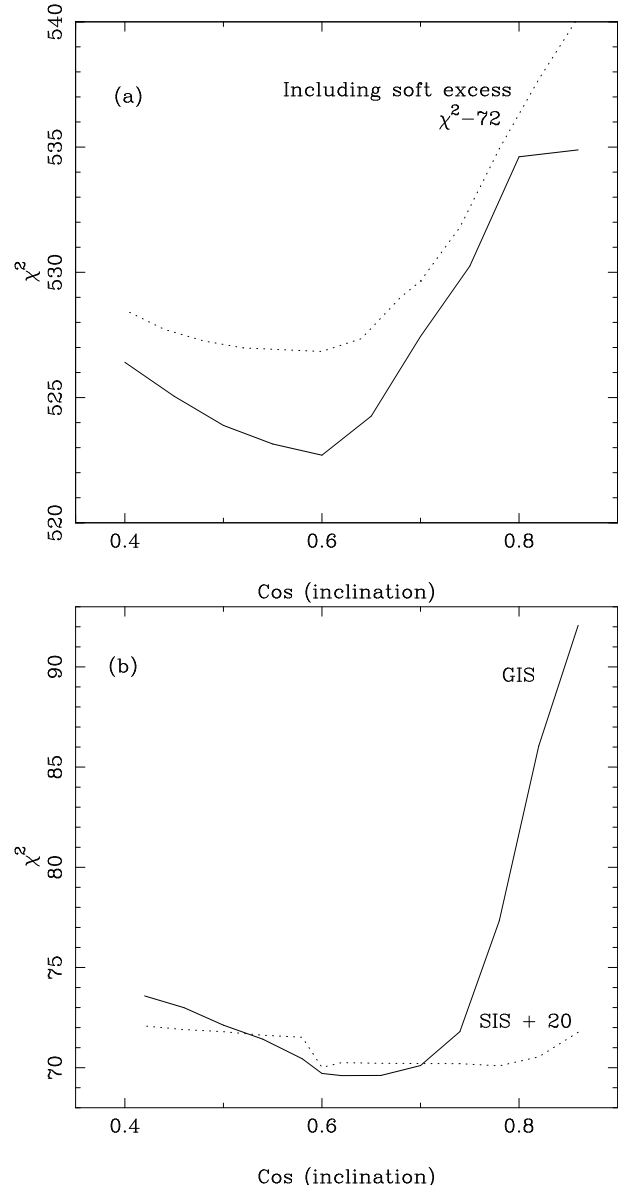


Figure 3. The change in χ^2 (goodness of fit parameter) as a function of inclination of the reflecting material. Panel (a) shows results from a simultaneous fit of all the EXOSAT GSPC spectra, with the solid line showing fits to the data from 4–20 keV while the dotted line uses the full 2–20 keV bandpass including a (diskblackbody) model for the soft excess. The latter have 72 subtracted from them in order to appear on the same scale. Panel (b) shows the ASCA GIS 3 (solid line) and ASCA SIS 5 (dotted line) 4–10 keV spectral results, where the latter have been boosted by 20 in order to appear on the same scale. Clearly the data which have significant bandpass beyond 9 keV favour inclinations higher than 30° .

the most probable inclination inferred from optical studies of $28^\circ - 38^\circ$ (Gies & Bolton 1986), but within the limit set by the most recent work of $\leq 55^\circ$ (Sowers et al 1998). At the best fit GSPC inclination of 53° the iron abundance is $2^{+0.6}_{-0.4} \times$ solar ($\chi^2_\nu = 522/604$). We check that this is not an artifact of ignoring the soft X-ray excess by including data down to 2 keV and approximating it with a diskblackbody

spectrum (XSPEC model `diskbb`). The dotted line in figure 3a shows that the data still significantly favour the higher inclination solutions.

Despite their higher spectral resolution, the ASCA SIS are completely unable to constrain the inclination (Figure 3b, dotted line). Figure 4a shows this degeneracy of SIS solutions in more detail. At low inclinations the data select uniquely the high ionization solution (shown in Figure 2), while at high inclinations an equally good solution can be found at both high and low ionization. Figures 5a and b show these high inclination solutions – the low ionization one has the ‘pseudo-edge’ in the data matched by the real edge while at high ionization it is matched by the drop from the broadened ionized line. Figures 5a and b also show the extension of these models out to 20 keV. It is obvious that these solutions can be distinguished with higher energy data.

The GIS data have just enough extra bandpass at high energies (above 9 keV) to break this degeneracy. The dashed line in figure 4b shows the change in χ^2 with ionization for $\cos i = 0.86$ and 0.6 for the GIS spectrum 3 of E96. Not only is the ionization uniquely determined for a given inclination, the data also are able to distinguish between the high ionization/low inclination and low ionization/high inclination solutions, clearly preferring the latter. The correspondence with the GSPC data is clear, so we fix the inclination of the relativistic reflector at 53° (cosine of 0.6) and re-fit all the data, using the best fit GSPC iron abundance of twice solar. These results are shown in Table 2. For the EXOSAT GSPC (and GINGA) data the fits are only subtly different – the derived ionization state is somewhat lower while the inner radius is somewhat larger, both because of the stronger doppler effects in the higher inclination models. However, for the ASCA data the high inclination solutions are very different from those in Table 1. Firstly, they are statistically better – the total χ^2 from all the GIS data for the high inclination solution is 698.5/632 as opposed to 753.4/632 for the low inclination one. Secondly, the derived ionization drops dramatically, and now corresponds to that seen in the EXOSAT GSPC data. All the data now give similar derived parameters, irrespective of bandpass. Only the SIS 5 and GIS 6 spectra allow a high ionization solution.

Unlike the variable gain EXOSAT GSPC data, the GIS data are all taken in the same mode, so their spectral residuals can be co-added in order to illustrate the features which make one model better than another. The data are fit simultaneously, with only the reflection parameters of iron abundance (constrained to be between 1–2× solar) and inclination fixed between the datasets. The top panel in Figure 6 shows the results from fitting a reflector which is ionized but not relativistically smeared for an inclination of 30° . There are clear broad residuals present around the iron line energy. A much better fit is obtained if the 30° ionized reflector is allowed to be relativistically smeared (and a non-smeared, un-ionized reflector is also added), as shown in the middle panel. However, the bluest features of the residuals are not able to be adequately fit in these models, despite the rather high derived ionizations (see table 1), due to the predominant redshift at 30° . Higher inclination solutions give a stronger doppler shift to the line, so matching the data rather better (bottom panel).

For the high inclination solutions, all the data show that the covering fraction of the relativistic reflector is al-

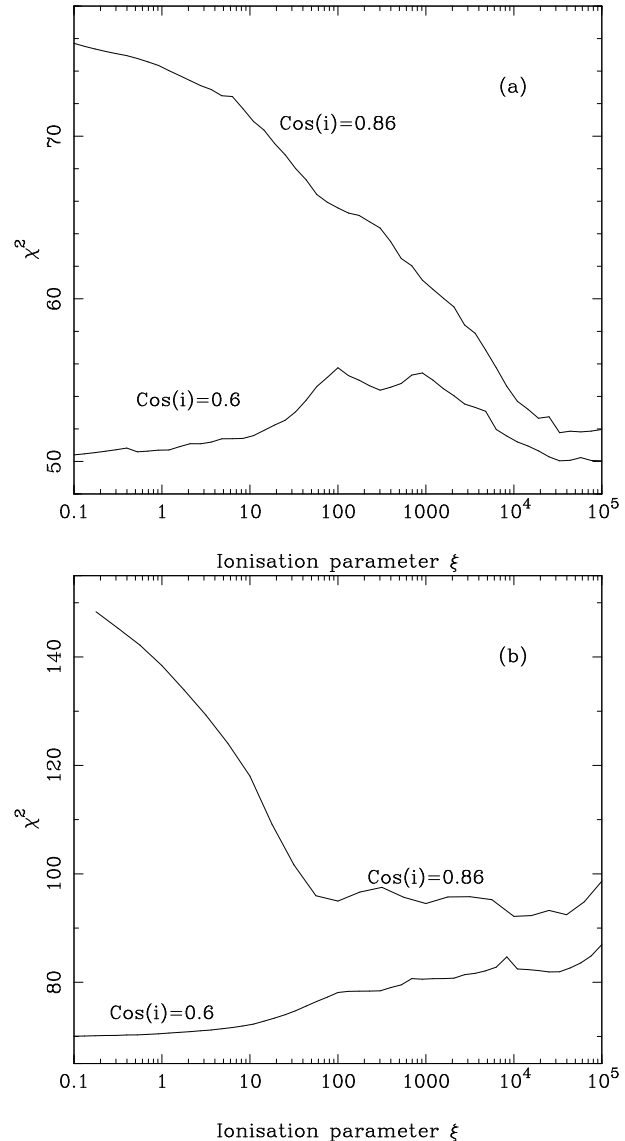


Figure 4. The change in the goodness of fit parameter χ^2 as a function of ionization state of the reflector for inclinations of 30° and 53° . Panel (a) shows the results for the SIS 5 spectrum. For an inclination of 30° the data uniquely select the high ionization solution while at 53° there are equally good solutions at both low and high ionization. All these three solutions are of comparable statistical likelihood. Panel (b) shows the contrasting situation derived from the GIS 3 spectrum. Here the data uniquely select the high inclination, low ionization solution.

ways much less than unity, the derived inner disk radius is generally significantly larger than $6R_g$, and its ionization state is rather low. The solid angle subtended by the narrow reprocessor is always consistent with being the $\Omega/2\pi \leq 0.1$ expected from the companion star. This should vary with orbital phase (Basko 1978), although the data here give error bars on the derived parameters which are too large to constrain this. Orbital variability in the narrow reflected component would provide an explanation for the observed 4% peak to peak quasi-sinusoidal variability seen in the high energy BATSE (20–100 keV) lightcurve of Cyg X-1 (Paciesas et al 1997). The reflected component should be small (bas-

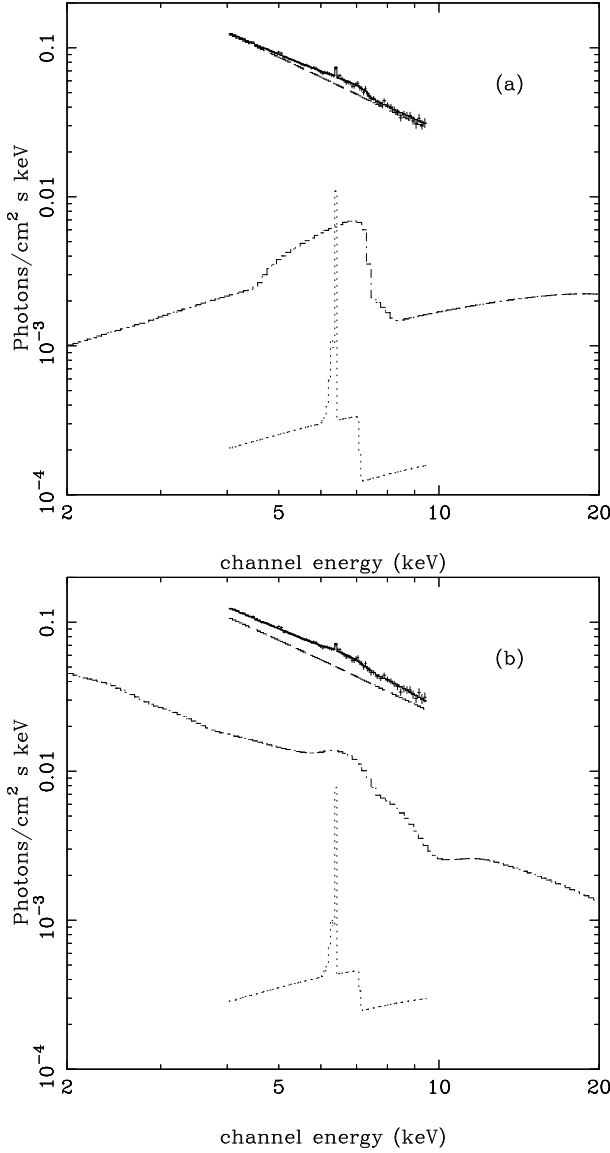


Figure 5. Two equally acceptable decompositions of the SIS 5 spectrum of Cyg X-1, assuming an inclination of 53° with iron abundance free to vary. Panel (a) shows the low ionization reflected continuum, with a relativistic disk of ionization $\xi = 0.04^{+0.25}_{-0.04}$, $R_{in} = 14 \pm 4$ and $\Omega/2\pi = 0.45^{+0.80}_{-0.10}$ ($\chi^2_\nu = 49.7/69$), for an illuminating power law with $\alpha = 0.73^{+0.16}_{-0.04}$ and neutral unsmeared reflection $\Omega/2\pi = 0.05^{+0.10}_{-0.03}$. The iron abundance is completely unconstrained between 0.5 – 3× solar. Panel (b) shows the high ionization solution, where the relativistic disk has $\xi = 3^{+34}_{-2.6} \times 10^4$, $R_{in} = 55^{+60}_{-30}$ and $\Omega/2\pi = 0.18^{+4.0}_{-0.11}$, with $\Omega/2\pi = 0.07 \pm 0.06$ of unsmeared neutral reflection and a power law with $\alpha = 0.70 \pm 0.04$ ($\chi^2_\nu = 50.0/69$).

cally zero) at phase 0 when the companion star is in front of the black hole, and have its maximum of $\Omega/2\pi \sim 0.1$ viewed at an inclination of $90 - i$ at phase 0.5, giving a 5% peak-to-peak variability in the 20–100 keV flux. We do not require an additional narrow reflected component from the outer disk, contrary to the conclusions of E96. Their fits to these data gave some spectra which required a much larger narrow component than could easily be explained by the companion star alone (e.g. GIS data from November 1994, spectrum

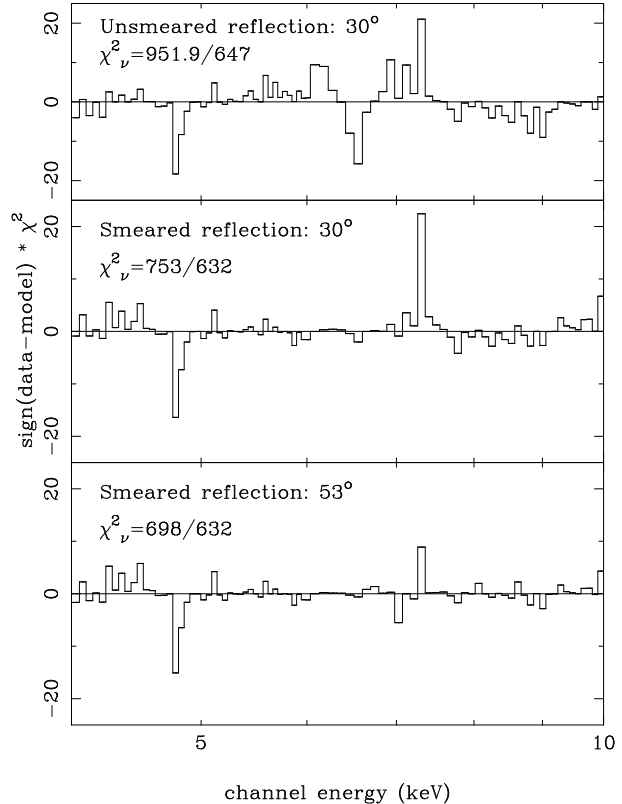


Figure 6. Co-added χ^2 residuals from fitting the 8 GIS spectra. The top panel shows results from fitting non-smeared reflection to the data. There are clearly broad residuals left around the iron line energy. The mid panel shows that these are much reduced by allowing the reflector to be a relativistic disk (including non-smeared, unionized reflection from the companion star). However, for the assumed inclination of 30°, the highest energy residuals are not matched by the models. The lower panel shows that these can be fit at higher inclinations, where doppler blueshifts can become stronger than the prevailing redshifts. The feature at 4.7 keV in all the plots is a residual from the changing response of the GIS detectors at the Xe L edge.

10), even allowing for twice solar iron abundances. The reason for the difference is that the fit is somewhat sensitive to changes in the model, and we note that our description gives better χ^2 (by up to 20) than the fits of E96.

4 IONIZATION AS A FUNCTION OF RADIUS

The data clearly prefer a solution in which the covering fraction of the reflector is extremely low, typically only 20–30 per cent of what would have been expected from a disk which covered half the sky as seen from the X-ray source, and the derived inner radius is generally inconsistent with the last stable orbit. Both these results can easily be explained in a scenario where the optically thick disk terminates before the last stable orbit, with the inner radii instead being filled with X-ray hot optically thin(ish) plasma. However, a series of papers (e.g. Ross et al 1996) have explored the possibility that high ionization of the reflector suppresses the derived amount of reflection. We have shown above that this does not work for Cyg X-1 when the reflector is modelled by

Table 2. EXOSAT GSPC, GINGA and ASCA data from Cyg X-1. Error bars are $\Delta\chi^2 = 2.7$, Galactic column is fixed at $6 \times 10^{21} \text{ cm}^{-2}$, inclination is 53° and the iron abundance is $2 \times$ solar

dataset	PL Γ	PL Norm	$\Omega/2\pi_{\text{rel}}$	ξ	R_{in}	$\Omega/2\pi_{\text{non-rel}}$	χ^2_ν
GSPC 08	1.77 ± 0.02	1.65	$0.34^{+0.05}_{-0.14}$	$0.2^{+17}_{-0.2}$	30^{+18}_{-11}	$0^{+0.14}_{-0.14}$	86.1/118
GSPC 09	$1.58^{+0.02}_{-0.01}$	1.28	$0.26^{+0.09}_{-0.12}$	$0^{+0.3}_{-0.3}$	28^{+22}_{-15}	$0.05^{+0.11}_{-0.05}$	96.3/98
GSPC 10	$1.58^{+0.02}_{-0.01}$	1.16	$0.13^{+0.05}_{-0.07}$	21^{+70}_{-20}	1000^{+970}_{-970}	$0^{+0.13}_{-0.13}$	69.7/104
GSPC 13	$1.78^{+0.02}_{-0.03}$	2.46	$0.34^{+0.12}_{-0.13}$	0^{+3}_{-3}	15^{+15}_{-9}	$0.09^{+0.10}_{-0.09}$	172.6/176
GSPC 14	$1.74^{+0.01}_{-0.02}$	1.85	0.39 ± 0.06	$0^{+0.4}_{-0.4}$	14^{+7}_{-4}	$0^{+0.05}_{-0.05}$	98.0/109
GINGA 91-1	1.63 ± 0.03	1.60	$0.33^{+0.15}_{-0.09}$	4^{+30}_{-4}	$40^{+\infty}_{-30}$	$0.1^{+0.1a}_{-0.1a}$	12.1/21
GINGA 91-2	1.63 ± 0.03	1.92	$0.44^{+0.10}_{-0.21}$	3^{+45}_{-3}	$30^{+\infty}_{-22}$	$0^{+0.1a}_{-0.1a}$	8.8/21
GIS 1	1.91 ± 0.02	1.89	$0.36^{+0.12}_{-0.13}$	$2.8^{+40}_{-2.7}$	20^{+6}_{-5}	$0.01^{+0.04}_{-0.01}$	93.5/79
GIS 3	1.91 ± 0.02	2.08	$0.53^{+0.09}_{-0.17}$	$0.02^{+17}_{-0.02}$	$9.9^{+6}_{-1.9}$	$0.08^{+0.03}_{-0.04}$	69.8/79
GIS 4	1.74 ± 0.02	1.28	0.31 ± 0.08	0^{+1}_{-1}	6.0^{+2}_{-2}	0.09 ± 0.03	134.4/79
SIS 5	1.74 ± 0.04	1.46	$0.54^{+0.17}_{-0.13}$	0^{+20}_{-20}	13^{+4}_{-3}	0.05 ± 0.03	49.9/70
GIS 6	$1.69^{+0.03}_{-0.02}$	1.94	$0.10^{+0.17}_{-0.09}$	30^{+1e5}_{-30}	18^{+30}_{-12}	0.12 ± 0.03	81.4/79
GIS 7	1.50 ± 0.03	1.01	$0.48^{+0.07}_{-0.11}$	0^{+10}_{-10}	14^{+5}_{-4}	$0^{+0.02}_{-0.02}$	45.7/79
GIS 8	$1.66^{+0.02}_{-0.01}$	1.45	$0.09^{+0.05}_{-0.07}$	50^{+2000}_{-45}	60^{+170}_{-44}	$0.05^{+0.05}_{-0.04}$	108.4/79
GIS 9	1.58 ± 0.02	1.42	$0.04^{+0.13}_{-0.04}$	$0^{+\infty}_{-1}$	$51^{+\infty}_{-45}$	$0.12^{+0.04}_{-0.12}$	71.7/79
GIS 10	1.61 ± 0.02	1.63	$0.04^{+0.09}_{-0.02}$	700^{+1700}_{-680}	100^{+220}_{-66}	$0.09^{+0.04}_{-0.05}$	93.6/79

^a Parameter restricted to the range 0–0.1 since it is not well constrained

Table 3. GSPC 08, SIS 5 and GIS 3 spectra fit to the radial ionization model with $\xi(r) \propto r^{-1.5}$. Error bars are $\Delta\chi^2 = 2.7$, Galactic column is fixed at $6 \times 10^{21} \text{ cm}^{-2}$. Inclination is fixed at 30° and 53° for each spectrum, while the iron abundance is allowed to vary between $1\text{--}2 \times$ solar (so there is an extra degree of freedom compared to table 2).

Spectrum	PL Γ	A_{Fe}	$\text{Cos}(i)$	$\Omega/2\pi_{\text{rel}}$	$\xi(R_{\text{in}})$	R_{in}	$\Omega/2\pi_{\text{non-rel}}$	χ^2_ν
GSPC 08	$1.77^{+0.01}_{-0.03}$	2.0	0.60	$0.34^{+0.04}_{-0.14}$	2^{+50}_{-2}	27^{+17}_{-8}	$0.01^{+0.12}_{-0.01}$	86.2/117
GSPC 08	1.77 ± 0.04	1.2	0.86	$0.22^{+0.04}_{-0.03}$	65^{+160}_{-56}	20^{+13}_{-7}	$0^{+0.09}_{-0.09}$	88.5/117
GIS 3	$1.91^{+0.09}_{-0.02}$	2	0.60	$0.53^{+0.40}_{-0.11}$	$0.01^{+11}_{-0.01}$	$9.5^{+3}_{-2.5}$	$0.09^{+0.07}_{-0.04}$	69.7/78
GIS 3	$1.85^{+0.01}_{-0.02}$	2	0.86	0.06 ± 0.01	$3.0^{+2.1}_{+3.5} \times 10^4$	34^{+27}_{-12}	$0^{+0.06}_{-0.06}$	89.7/78
SIS 5	$1.75^{+0.13}_{-0.04}$	2	0.6	$0.56^{+0.59}_{-0.12}$	$0.1^{+30}_{-0.1}$	$13^{+6}_{-3.5}$	$0.06^{+0.08}_{-0.03}$	49.4/69
SIS 5	$1.69^{+0.05}_{-0.03}$	2	0.6	$1.08^{+\infty}_{-0.99}$	$1.40^{+2.1}_{-1.37} \times 10^6$	17^{34}_{-10}	$0.11^{+\infty}_{-0.06}$	50.7/69
SIS 5	$1.67^{+0.05}_{-0.03}$	2	0.86	$0.11^{+\infty}_{-0.06}$	$1.8^{+38}_{-1.5} \times 10^5$	14^{+16}_{-6}	$0.05^{+\infty}_{-0.04}$	52.0/69

material with constant ionization parameter. However, perhaps there is a radial range of ionization states. If there is an extremely ionized inner disk then it produces no spectral features, so neither its covering fraction nor its relativistic smearing can be seen.

We test this idea by dividing the disk into 10 radial zones, again with the illumination $\propto r^{-3}$, and the ionization $\xi(r) \propto r^{-1.5}$ as appropriate for a gas pressure dominated disk. Due to computational time we only demonstrate this model on a single spectrum from each instrument: EXOSAT GSPC 08, ASCA GIS 3 and ASCA SIS 5. The iron abundance is a free parameter (within the range $1 - 2 \times$ solar), and we include the possibility of a neutral reflected component from the star/outer disk. The fits are repeated for fixed inclination of $\cos i = 0.6$ and 0.6.

Details are given in Table 3, and are not significantly different from those derived from the single ionization model. The inferred covering fraction for the disk is still low, and the disk inner radius is inconsistent with the last stable orbit. We explicitly searched for a high ionization solution for the $\cos i = 0.6$ fits, but these always gave a significantly worse χ^2 except for the SIS 5 data.

The reason for the failure of the multi-zone ionization model is that the mean ionization state observed is rather low. Between this and the extreme ionization states required to make the reflector invisible are the intermediate/high ionization states. These give a strong and distinctive spectral signature, especially those where iron has only one or two electrons left (H and He-like, FeXXVI and XXV) which produce intense line emission at 7.0 and 6.7 keV, and (more importantly) a deep edge at 9.2 and 8.6 keV (Ross & Fabian 1993). Even allowing for strong distortion by relativistic smearing (Matt et al., 1993a; 1996; Ross et al., 1996) these features are not seen in the data. It is not then possible to go smoothly from the observed rather low ionization states to the extreme ionizations required to hide reflection. Only if there is an abrupt ionization transition can this model be sustained.

Again, we note that good data at energies ≥ 9 keV are required in order to constrain the amount of highly ionized reflecting material. Radial ionization models with high inner disk ionization can be fit to the SIS data for any inclination, but are again ruled out by the GIS 3 spectrum (see table 3).

5 DISCUSSION

From the above fits it is clear that the relativistic smearing of the reflected spectrum is significantly detected in Cyg X-1, confirming the presence of an optically thick material at small radii – the putative accretion disk. The covering fraction of the disk is substantially less than unity (see Tables 1-3), irrespective of inclination, ionization and radial gradients in ionization.

The ionization of the reflector and its inclination to the line of sight can be constrained with moderate spectral resolution data *and* bandpass extending beyond 9 keV. The data show strong preference for a low ionization reflector inclined at rather more than 30° to the line of sight: the ASCA GIS 3 spectrum gives a range of $41^\circ - 61^\circ$, while the EXOSAT GSPC data imply angles greater than $\sim 47^\circ$ (both at the 90% confidence limit). These inclinations are determined by the detailed shape of the iron line in the data: for low inclinations the theoretical line profile is strongly affected by gravitational redshift so that higher ionization solutions are needed to fit the data. But in higher ionization solutions there is a large energy separation between the line and edge (however smeared they become) which is *not* seen in the data. The spectral features observed require that the line and edge blend together, i.e. that the ionization is moderate to low. The reflector then is required to be viewed at a moderate inclination angle so that the doppler blueshift can counteract the gravitational redshift. However, these inclinations are rather larger than the often quoted probable range of $28^\circ - 38^\circ$ (Gies & Bolton 1986) derived from optical data, although within the firm upper limit to the inclination from these studies of $i \leq 55^\circ$ (Sowers et al 1998). The lack of a well determined optical orbital solution is due to the complexity of the accretion flow from the supergiant companion in this system. The companion probably does not completely fill its Roche lobe, but instead has a strong stellar wind which is gravitationally focussed by the Roche potential (see e.g. numerical simulations by Blondin, Stevens & Kallman 1991)

While the iron line is strongly distorted by the relativistic effects, the extremely broad components from material at $6R_g$ are not present at the level expected from a disk extending down to the last stable orbit with line emissivity $\propto r^{-3}$. Such a model is only possible if the inner disk has an *abrupt* increase in ionization state to the level at which it becomes completely ionized so produces no atomic spectral features. We stress that a continuous (power law) ionization gradient as expected from the intense X-ray illumination is insufficient to do this, since between the observed rather low ionization state of the reflector and the extreme ionizations required to make the disk completely reflective there are the high ionization states, where iron has only 1 or 2 electrons left. These ions produce copious $K\alpha$ line emission at 6.7 and 7.0 keV, and strong edges at 8.8 and 9.2 keV, which are not seen in the data. Similarly, these high ionization states are precisely the ones expected from collisional ionization from the accretion disk temperature. The observed soft excess is dominated by a component at 0.1 – 0.2 keV which cannot completely ionize iron. Even the secondary soft emission at $kT \sim 1$ keV is far removed from the inner K shell energy of 8.8 and 9.2 keV for He and H like iron. This then rules out the idea of a simple correspondence between AGN and GBHC where both have disks which extend down to $6R_g$

but in the GBHC the disk is ionized simply because of the higher accretion disk temperature.

The optically thick disk must do *something* at the derived $R_{\text{in}} > 6R_g$ (assuming that the line emissivity is $\propto r^{-3}$; Życki et al 1998b). Either the inner disk disappears completely or it jumps *discontinuously* to a completely ionized state at this radius. Similar results are seen for the low/hard state GBHC transient sources (Życki et al 1997; 1998ab), showing that this is a robust feature of low/hard state GBHC spectra.

Figure 7 shows the plot of spectral index versus the derived covering fraction, ionization and inner radius of the reflector for the reflector models inclined at 53° (not including the poorly constrained GINGA data). The covering fraction is not consistent with a constant ($\chi^2_\nu = 60/14$), showing that the geometry must be changing. Apart from the hardest spectral index data (GIS 7, which incidentally is the spectrum taken furthest off axis, and so has a large vignetting correction, E96) the data are consistent with a trend in which a hard spectral index is associated with smaller reflected fraction, similar to results from some of the X-ray transients (Życki et al 1997; 1998ab). This can be qualitatively explained by a geometry in which there is a variable radius inner hole in the cool disk which is filled with X-ray hot plasma, although the error bars on the radius derived from relativistic smearing are too large to be able to constrain these ideas. A disk which extends further down into the gravitational potential could subtend a larger solid angle to the source. The soft photon flux from the disk would also increase, both because the disk luminosity is dependent on its inner radius, and also from the larger fraction of hard X-rays which can be reprocessed. This would give stronger Compton cooling of the hot electrons and so a steeper X-ray spectrum.

The typical derived inner radius of the disk is $R_{\text{in}} = 20R_g$. The luminosity released by viscous dissipation from $20R_g$ to $6R_g$ is rather less than 0.75 that released from ∞ to $20R_g$ (see e.g. equation 5.19 in Frank, King & Raine 1992). Simple energetics then give the expectation that the X-ray hot plasma should carry $\sim 0.75 \times$ the luminosity of the soft photons from the disk. However, the opposite is observed: the hard component (the X-ray hot plasma) is over twice as luminous as the soft component from the disk e.g. di Salvo et al., (1998).

However, this geometrical interpretation is clearly not unique, and many others have been proposed (see e.g. the review by Poutanen 1998). If the hot X-ray emitting plasma forms a (plane parallel) corona above the disk (e.g. Haardt & Maraschi 1993) then the reflected spectrum has to cross the corona before escaping to the observer. A fraction $\exp(-\tau/\cos i)$ (where τ is the optical depth and i the inclination of the disk–corona to the observer) will interact again with the hot electrons in the plasma. The reflected spectrum then forms another source of seed photons for Compton scattering, and the scattered fraction joins the Compton continuum and so is unrecognisable as reflected flux. Such models were shown to work for Cyg X-1 data up to 20 keV (Haardt et al 1994), but they predict that there should be a strong break in the spectrum beyond this energy. Seed photons from the disk are not isotropic, so the first few Compton scattering retain the imprint of this anisotropy and give a somewhat flatter spectrum which then joins onto the more

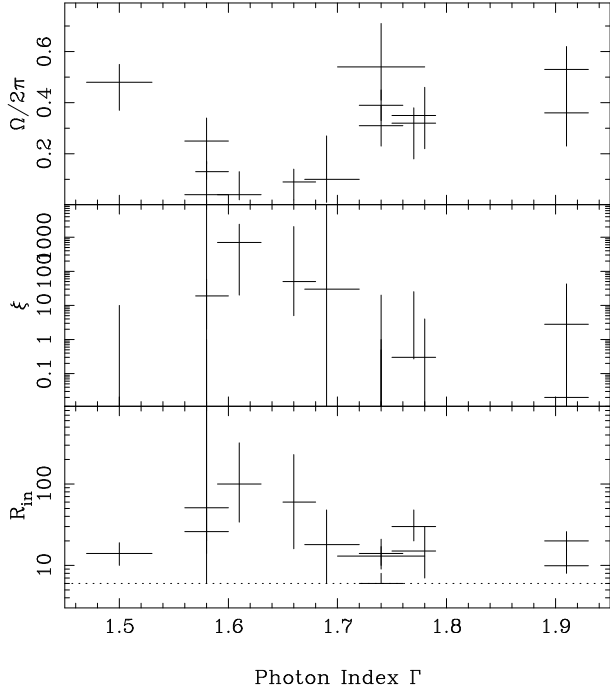


Figure 7. The relativistic reflection spectrum parameters as a function of the intrinsic spectral index for the model with reflector inclination of 53° (table 2). The top panel shows the amount of reflection, while the second panel shows its ionization state and the third shows its inner radius.

isotropic higher order scatterings (Haardt & Maraschi 1993). This anisotropy break is *not* present in broad band spectra from Cyg X-1, where the data extend past 20 keV, which rules out such models (Gierliński et al 1997a).

The lack of an anisotropy break seems to be an insurmountable problem for any model which has the X-ray emission region above a disk, including the ‘active regions’ models which may be more appropriate if the X-ray regions are energised by localised magnetic reconnection events (e.g. Haardt, Maraschi & Ghisellini 1994). However, these models are very attractive given that accretion disk viscosity is now thought to be driven by magnetic reconnection. But even if the anisotropy break can be masked (perhaps by the electrons also being anisotropic or by a distribution of electron temperatures) there are further problems for models where the X-ray region is above the disk. If edge effects are not important (approximately plane parallel geometry) then about half of the hard X-rays are intercepted by the disk. The majority (whatever is not reflected) of this flux is thermalised in the disk and re-emerges as soft photon seeds for the Compton scattering. These soft photons all have to pass through the corona in a plane parallel geometry, resulting in strong cooling. Without a strong anisotropy break then the predicted spectra are too soft to match the observed low/hard spectra from Cyg X-1 (Dove et al 1997, Poutanen et al., 1997). This forces us to the ‘active regions’ models, where not all flux of soft photons from the disk will pass through the corona as edge effects are important. But in these models there is then no overlying corona that can reduce the amount of reflection seen. If edge effects are important, then much of the reflection is produced from regions of the disk that are not underneath the corona. Reflection is not then su-

pressed by Compton scattering in the corona, and there is the strong prediction that we should see $\Omega/2\pi_{\text{rel}} = 1$, which is plainly not the case.

These are serious problems to be faced by all models which have the X-ray region above the disk. The continuous disk—corona models can reduce the amount of reflection seen, but predict a large anisotropy break which is strongly ruled out by the data. Even if there is some way to mask the anisotropy break then these models produce spectra which are too soft to match what is seen. The ‘active regions’ models can produce hard spectra, but cannot suppress reflection and again predict an anisotropy break which is not seen. Compared to these drawbacks, the central source geometry seems an attractive option.

6 EQUILIBRIUM ACCRETION FLOW SOLUTIONS

There are several solutions of the equations for accretion of material onto a compact object. The most well known of these is that of Shakura & Sunyaev (1973; hereafter SS), which is the geometrically thin, optically thick accretion disk. In this solution, the gravitational energy released is radiated away locally as (quasi)blackbody radiation. However, other solutions are also possible: the energy can instead be radiated by Compton scattering in an optically thin(ish), geometrically thick(ish) flow (Shapiro, Lightman & Eardley 1976). Alternatively, the energy released need not be efficiently radiated. It can be carried along with the flow (advected) and swept into the black hole. These inefficient, advectively cooled flows can either be optically thin (ADAFs: Narayan & Yi 1995; Abramowicz et al 1995), or optically thick (Abramowicz et al 1988), depending on the mass accretion rate. In general the solutions coexist: at any radius there are several different equilibrium flow configurations for a given mass accretion rate and viscosity (see e.g. Chen et al., 1995).

6.1 Shakura–Sunyaev Accretion

Why should the inner disk radius change, and not extend down to $6R_g$? The ‘standard’ accretion disk model developed by SS gives the flow structure in the limit when the gravitational energy is released in optically thick material. The cooling is very efficient (blackbody radiation), so all the energy released locally can be radiated locally, giving a cool, geometrically thin disk structure. This becomes unstable when the total pressure is dominated by radiation pressure (Shakura & Sunyaev 1976), giving a natural inner disk cutoff. For steady state models these predict that the inner radius should move outwards as the luminosity increases (as the radiation pressure dominated region increases: SS), in conflict with the observed trend in the transient GBHC to show higher reflected fractions and smaller inner disk radii at higher luminosities (Zyczyński et al 1997; 1998a,b).

Another, more general problem with the SS accretion disk structures is that such models give temperatures of order 1 keV for GBHC at high accretion rates but are quite unable to explain the observed (hard or soft) power law tail out to energies ≥ 100 keV. Either there are parts of the disk flow in a different configuration to that of SS, or

there is some non-disk structure such as a corona powered by magnetic reconnection (e.g. Haardt, Maraschi & Ghisellini 1994). However, this latter possibility (a cool disk underneath a plane parallel or hemispherical X-ray emitting corona) seems to be ruled out by detailed spectral fitting (see Section 6). Instead it seems that the spectrum implies a geometrical constraint that the X-ray emitting plasma and disk occupy more or less separate regions, such as an outer disk and inner (quasi-spherical?) X-ray source (Gierliński et al 1997a, Dove et al 1997, Poutanen et al., 1997).

6.2 Advective Accretion

Recently there has been much excitement about the possibility that another stable solution of the accretion flow may explain the hard X-ray data. Below a critical accretion rate, $\dot{m} \leq \dot{m}_{\text{crit}}$, a stable, hot, optically thin, geometrically thick solution can be found if radial energy transport (advection) is included (see e.g. the review by Narayan 1997). The key assumption of these models is that the protons gain the energy from viscous processes, while the electrons only acquire energy through interactions (electron-ion coupling) with the protons. This coupling timescale can be rather slow compared to the accretion timescale, so protons can be accreted into the black hole, taking some of the energy with them. The energy that the electrons do manage to obtain is radiated away via cyclotron/synchrotron emission (on an internally generated magnetic field), bremsstrahlung, or Compton scattering of the resultant spectra of these two processes. In contrast to the SS accretion flow models, there is no cold disk in the inner regions, so no strong source of soft seed photons for Compton scattering, hence the resulting X-ray spectra are typically hard.

Such flows were proposed to explain the hard and very faint X-ray spectra seen from the transient X-ray GBHC in quiescence (e.g. Narayan, McClintock & Yi 1997), and then extended by Esin, McClintock & Narayan (1997) to cover the whole range of luminosity seen in the GBHC transients. As the mass accretion rate increases from $\dot{m} \ll \dot{m}_{\text{crit}}$ to $\dot{m} \sim \dot{m}_{\text{crit}}$ the flow density increases, so the electron-ion coupling becomes more efficient and the fraction of energy the electrons can drain from the protons increases. This increase in radiative efficiency continues to $\dot{m} = \dot{m}_{\text{crit}}$, where only $\sim 35\%$ of the heat energy is advected. At higher $\dot{m} > \dot{m}_{\text{crit}}$ the advective flow collapses into an SS disk. Esin et al (1997) identify this change from a hot advective flow to a cool SS disk as the origin of the hard / soft spectral transition seen in GBHC, and some observational support for this is indeed seen (Życki et al., 1998a, Cui et al., 1998, Gierliński et al., 1997b).

These models have been specifically applied to Cyg X-1 by Esin et al (1998). Their calculated spectra approximately match the overall 2–500 keV GINGA–OSSE data from Cyg X-1 for $R_{\text{in}} \sim 200R_{\text{g}}$, but uncertainties in their model may extend this to $R_{\text{in}} \geq 40R_{\text{g}}$. This is still larger than most of the constraints from relativistic smearing (table 2). Our data indicate that the optically thick material extends much further into the gravitational potential than anticipated by the advective flows. Similar results are found for the comparison of the models of Esin et al (1997) against the observed hard state spectra from the GBHC transient source Nova Muscae (Życki et al., 1998a).

6.3 Shapiro–Lightman–Eardley flows

An alternative X-ray hot solution to the cool SS accretion flow was discovered by Shapiro et al., (1976, hereafter SLE). These solutions are actually very closely related to the ADAFs discussed above in that they assume that the protons gain most of the energy from viscous processes, and then heat the electrons by electron-ion coupling, resulting in an optically thin(ish), geometrically thick(ish) flow. This solution of the accretion flow equations merges into the ADAF branch at a critical mass accretion rate (see Chen et al 1995; Esin et al 1997; Zdziarski 1998). The key difference is that on the SLE branch, Compton cooling dominates over advection, while the opposite is true on the ADAF branch. There is no known possible hot solution for mass accretion rates above the critical one at which the ADAF and SLE solutions merge.

In its original form, the SLE solutions were shown to be viscously stable but thermally unstable (Pringle 1976). An increase in the heating rate is not balanced by an increase in the cooling because the electron-ion collisions become less efficient as the temperature increases. The key to the growth of interest in ADAFs is that they are stabilized against this due to the dominance of advective cooling. However, the SLE is not *necessarily* thermally unstable. The stability analyses which have been done generally assumed that the viscous timescale is long compared to the thermal timescale, so that the density of the region cannot change during the perturbation. This is not true for a geometrically thick(ish) flow. Many stability analyses also neglected advective cooling, and/or external Compton cooling on seed photons which vary. We urge further study of the thermal stability of these flows.

Understanding the stability (and hence the existence) of these flows is important since the SLE composite geometry is rather similar to that inferred from the data, with a hot, quasi-spherical plasma cooled by radiation from an external SS accretion disk. The advantage the SLE solution has over the ADAF is that it radiates efficiently, which is generally required from the rapid observed variability of accreting black holes. However, the disk transition again occurs where radiation pressure dominates over gas pressure, so these models again apparently predict that the inner disk radius is larger at high mass accretion rates, opposite to the observed trend.

7 UNSTABLE ACCRETION IN AN SS DISK

The thermal instability above is produced wherever an increase in the mass accretion rate is not balanced by a corresponding change in the cooling rate. Similarly, a disk is viscously unstable if a small increase in the external mass accretion rate cannot be balanced by the viscosity to produce a corresponding change in the mass accretion rate through the disk. These two are related in that flows which are viscously unstable are also necessarily thermally unstable.

The ionization of Hydrogen produces a disk transition which is viscously (and thermally) unstable. Below temperatures of ~ 5000 K the opacity is dominated by molecular lines, while above this temperature there is a marked increase in opacity due to bound-free ionization of Hydrogen. However, for temperatures beyond $\sim 10^4$ K the bound-free

opacity drops since hydrogen is then mostly ionized. This gives a local maximum in opacity at $\sim 6000 - 10^4$ K (e.g. Hure et al 1994). In this range an increase in \dot{m} gives rise to a large increase in opacity, trapping the radiation and raising the central (equatorial plane) temperature of the disk. This in turn raises the sound speed, c_s , and the kinematic viscosity, $\nu = \alpha c_s H$, leading to an increase in the rate at which the disk material is accreted onto the compact object (see e.g. the review by Osaki 1996).

If this instability can propagate throughout the disk then this leads to two distinct states. In quiescence the disk is cool and has low kinematic viscosity – generally so low that the rate at which material is added to the disk from the external accretion source is faster than the rate at which mass can be viscously transported inwards from the outer disk. Mass builds up at the outer edge of the disk, and the structure is *not* that of a cool steady SS disk. Eventually, the outer disk mass is so large that hydrogen can be ionized, and then the disk switches to a hot state where the kinematic viscosity is high and steady state can be achieved.

This instability is thought to be the trigger for the outburst in the transient black hole systems (see e.g. Lasota, Narayan & Yi 1996), though it was first discovered in the context of the quiescent/outburst behaviour of disk accreting white dwarfs (see e.g. the review by Osaki 1996). However, one major problem with these models is that the accretion rate inferred in quiescence (as evinced by the X-ray emission) is rather larger than the maximum accretion rate for which the cool quiescent disk can be sustained if the disk extends all the way down to the compact object (Lasota et al., 1996). This led to the idea of a ‘hole’ in the inner disk in quiescence, perhaps formed by evaporation (Meyer & Meyer-Hofmeister 1994). However, another possibility which has yet to be explored in this context is that the inner disk in quiescence is simply optically thin. The surface density profile for the non-stationary cool quiescent disk is peaked to the outside of the disk, so it is very easy for the inner regions to be optically thin (e.g. Cannizzo 1998, figure 7), especially as the *absorption* opacity of the cool disk is low so even if the photon is scattered many times, there is still a high probability that it can ultimately escape (effectively optically thin). This means that the inner disk is unlikely to be able to thermalise the energy released locally, and so may not radiate (i.e. cool) efficiently. The material would then heat up, and turn into something like an advective or externally cooled SLE flow which would appear to emanate from a (non stationary) optically thick disk.

However, the main problem with such models is that while this may describe the situation in quiescence, it seems highly unlikely that it has any relevance to the high mass accretion rates required for Cyg X-1 and the other X-ray bright transient GBHC. Another instability that can give the same effect but at high mass accretion rates is required. One obvious possibility is the instability which occurs when radiation pressure starts to dominate in the disk. The internal pressure (and hence the sound speed and kinematic viscosity) then rises very rapidly ($\propto T^4$), and the mass accretion rate through the radiation pressure dominated part of the disk can then increase faster than the increase in external mass accretion which triggered the rise in temperature, so leading to depletion of the inner disk. At higher mass accretion rates the flow is again stabilised though the

excess radiation being carried along with the flow and advected into the black hole (Abramowicz et al 1988). Models of such flows are beginning to be developed (Szuszkiewicz & Miller 1998) in response to observations of rapid inner disk instabilities in the superluminal accreting black hole candidate GRS1915+105 (Belloni et al 1997), but are currently in their infancy. It remains to be seen whether models of a non-stationary flow inside the radiation pressure dominated regime could reproduce what is seen in Cyg X-1 and other low state GBHC spectra.

8 INHOMOGENEOUS ACCRETION

It seems highly unlikely that accretion flow can change smoothly between an optically thick cool solution and an optically thin hot solution. Some transition region where cool clumps are embedded in hot plasma seems physically more probable, and turbulence is indeed seen in the numerical calculations of Abramowicz, Igumenshchev & Lasota (1998). Recent work on an inhomogeneous solution to the accretion flow equations has shown that there is a stable solution to the radiation pressure dominated SS disk if the majority of mass is in dense clumps which are optically thick, while the remainder forms an optically thin(ish), X-ray hot plasma (Krolik 1998), with a physical mechanism for clumping provided by the photon bubble instability (Gammie 1998). However, one problem with these models is that they seem to predict that the covering fraction of cool clumps is close to unity for stellar mass black holes, in conflict with the observations.

9 CONCLUSIONS

We detect significant relativistic smearing of the reflected spectral features in Cyg X-1, giving the first observational confirmation of an inner accretion disk in Cyg X-1. Our model calculates the total (line plus continuum) reflected spectrum for a given ionization state and iron abundance and then applies the relativistic smearing at a given inclination. These four parameters can be uniquely determined from X-ray spectra (assuming a given illuminating flux) with moderate energy resolution, and excellent signal-to-noise data extending beyond 9 keV. These conditions are satisfied in Cyg X-1 for the EXOSAT GSPC and ASCA GIS spectra. The GINGA data are taken in a reduced spectral resolution mode, while the ASCA SIS data have insufficient signal-to-noise above 9 keV.

For the ASCA GIS and EXOSAT GSPC data the reflected spectrum is constrained to be from material inclined at $\geq 45^\circ$ which is not highly ionized. The low ionization state rules out Auger ionization as a mechanism for suppressing the line with respect to the reflected continuum as proposed by Ross et al (1996). The iron line is not weak with respect to the reflected continuum – we infer twice solar iron abundance – but the visibility of the line is dramatically reduced by relativistic smearing.

The observed amount of relativistic smearing is not consistent with a disk extending all the way down to the last stable orbit around the black hole, but instead indicates that the disk truncates at some typical (but probably variable)

radius of $\sim 10 - 30R_g$, with a trend that larger transition radii are associated with harder X-ray spectra. This mirrors the results from the hard spectra of the transient GBHC such as V404 Cyg and Nova Muscae (Życki et al 1997; 1998ab), suggesting that low state can be associated with a lack of optically thick disk at the innermost radii.

The amplitude of the reflected component is significantly less than that expected from an isotropic source above a semi-infinite disk. Again this result can be understood in the context of an inner 'hole' in the optically thick material which is filled by the X-ray emitting plasma. Similar conclusions about the geometry are also found from looking at the detailed continuum spectral shape of Cyg X-1, where the hardness of the X-ray spectrum implies that the hot X-ray plasma is spatially separate from most of the accretion disk, otherwise it intercepts too many soft photons from the disk and produces an X-ray spectrum which is significantly steeper than observed (Gierliński et al 1997a; Dove et al 1997; Poutanen et al 1997).

The data then strongly indicate that low state GBHC accretion geometry is that of an inner X-ray hot, optically thin(ish), geometrically thick plasma, which cools by Compton upscattering of soft photons from an external cool, optically thick, geometrically thin disk. Such a composite flow seems most likely to be a standard SS cool outer disk, with an inner ADAF or SLE flow. The SLE flow is probably thermally unstable, so for steady state solutions the ADAF seems to be preferred. However, we stress that the radiation pressure instability may put the disk in a regime where the flow is not in steady state, or is inhomogeneous.

10 ACKNOWLEDGEMENTS

We thank Ken Ebisawa and Yoshihiro Ueda for kindly allowing us to use their Cyg X-1 ASCA data, Andrew King, Uli Kolb and Juri Poutanen for stimulating discussions, and Andrzej Zdziarski the referee for useful comments. CD acknowledges support from a PPARC Advanced Fellowship.

REFERENCES

Abramowicz M.A., Igumenshchev I.V., Lasota J.-P., 1998, MNRAS, 293, 443

Abramowicz M.A., Czerny B., Lasota J.-P., Szuszkiewicz E., 1988, ApJ., 332, 646

Abramowicz M.A., Chen X., Kato S., Lasota J.-P., Regev O., 1995, ApJL., 438, 37

Balucinska M., Hasinger G., 1991, A&A, 241, 439

Basko M.M., 1978, ApJ., 223, 268

Belloni T., Mendez M., King A.R., Van Der Klis M., Van Paradijs J., 1997, 488, 109

Blondin J., Stevens I., Kallman T.R., 1991, ApJ., 371, 684

Cannizzo J., 1998, ApJ., 494, 366

Chen X., Abramowicz M.A., Lasota J.-P., Narayan R., Yi, I., ApJL, 1995 443, 61

Cui W., Ebisawa K., Dotani T., Kubota, A., 1998, ApJ., 493, 75

Di Salvo T., Done C., Życki P., Burderi L., Robba N., In 'The Extreme Universe', Ed Winkler C., Gordon & Breach, in press.

Done C., Mulchaey J.S., Mushotzky R.F., Arnaud K.A., 1992, ApJ., 395, 275

Dove J., Wilms J., Maisack M., Begelman M.C., 1997, ApJ., 487, 759

Ebisawa K., Ueda Y., Inoue H., Tanaka Y., White, N.E. 1996, ApJ., 467, 419

Esin A. A., McClintock J.E., Narayan R., 1997, ApJ., 489, 865

Esin A.A., Narayan R., Cui W., Grove J.E., Zhang S-N., 1998, ApJ., 505, 854

Fabian A.C., Rees M.J., Stella L., White, N.E. 1989, MNRAS, 238, 729

Frank J., King A.R. & Raine D., 1992, In "Accretion power in Astrophysics", 2d edition, Cambridge, UK: Cambridge University Press

Gammie C., 1998, MNRAS, 297, 929.

George I.M., Fabian A.C., 1991, MNRAS, 249, 352

Gierliński M., Zdziarski A. A., Done C., Johnson W. N., Ebisawa K., Ueda Y., Philips F. 1997a, MNRAS, 288, 958

Gierliński M., Zdziarski A.A., Dotani T., Ebisawa K., Jahoda K., Johnson W.N., 1997b, in Proc. 4th Compton Symposium, eds Dermer C.D., Strickman M.S., Kurfess J.D., AIP 410, p844

Gies D.R., Bolton C.T., 1986, ApJ., 304, 371

Haardt F., Maraschi L., 1993, ApJ., 413, 507

Haardt F., Done C., Matt G., Fabian A.C., 1993, ApJL., 411, 95

Haardt F., Maraschi L., Ghisellini G., 1994, ApJ., 432, 95

Hure, J.-M., Collin-Souffrin S., Le Bourlot J., Pineau des Forets G., 1994, A& A., 290, 34

Iwasawa K., Fabian A.C., Mushotzky R.F., Brandt W.N., Awaki H., Kunieda H., 1996, MNRAS, 279, 837

Kaastra J.S., Mewe R., 1993, A&AS, 97, 443.

Kitamoto S., Miyamoto S., Tanaka Y., Ohashi T., Kondo Y., Tawara Y., Nakagawa M., 1984, PASJ, 36, 799

Krolik J.H., 1998, ApJL., 498, 13

Lasota J.-P., Narayan R., Yi I., 1996, A&A, 314, 813

Lightman A.P., White T.R., 1988, ApJ, 335, 57

Magdziarz P. Zdziarski A.A., 1995, MNRAS, 273, 837

Marshall F.E. Mushotzky R.F., Petre R., Serlemitsos P.J., 1993, ApJ., 419, 301

Matt G., Perola G.C., Piro L. 1991, A&A, 247, 25

Matt G., Fabian A.C., Ross R., 1993a, MNRAS, 262, 179.

Matt G., Fabian A.C., Ross R., 1993b, MNRAS, 264, 839

Matt G., Fabian A.C., Ross R., 1996, MNRAS, 278, 1111

Meyer F., Meyer-Hofmeister E., 1994, A&A, 288, 175

Morrison R., McCammon D., ApJ., 270, 119

Nandra K., Pounds K.A., 1994, MNRAS, 268, 405

Narayan R. 1997, in Proc. IAU Colloq. 163 on Accretion Phenomena and Related Outflows, eds. D. T. Wickramasinghe, L. Ferrario, G. V. Bicknell, p. 75

Narayan R., McClintock J. E., Yi I., 1996, ApJ, 457, 821

Narayan R., Yi I., 1995, ApJ., 444, 231

Osaki Y., 1996, PASP, 108, 39

Paciesas W.S., Robinson C.R., McCollough M.L., Zhang S.N., Harmon B.A., Wilson C.A., 1997, in Proc. 4th Compton Symposium, eds Dermer C.D., Strickman M.S., Kurfess J.D., AIP 410, p834

Pounds K.A., Nandra K., Stewart G.C., George I.M., Fabian A.C., 1990, Nature, 344, 132

Poutanen J., Krolik J.H., Ryde F., 1997, MNRAS, 292, L21

Poutanen J., 1998, In 'Theory of Black Hole Accretion', CUP, in press.

Pringle J., 1976, MNRAS, 177, 65

Reilman R.F., Manson S.T., 1979, ApJS., 40, 815

Ross R.R., Fabian A.C., 1993, MNRAS, 261, 74.

Ross R.R., Fabian A.C., Brandt W.N., 1996, MNRAS, 278, 1082

Shakura, N.I., Sunyaev, R.A. 1973, A& A, 24, 337

Shakura, N.I., Sunyaev, R.A. 1976

Shapiro S.L., Lightman A.P., Eardley D.M., 1976, ApJ, 204, 187

Sowers J.W., Gies D.R., Bagnuolo W.G., Shafter A.W., Wiemker R., Wiggs M.S., 1998, ApJ., 505, 424

Szuszkiewicz E., Miller J.C., 1998, MNRAS, 298, 888

Tanaka Y. et al. 1995, Nature, 375, 659

Zdziarski A.A., 1998, MNRAS, 296, L51

Zdziarski A.A., Lubinski P., Smith D.A., 1999, MNRAS, in press
Życki P.T., Done C., Smith D.A., 1997, ApJL, 488, 113
Życki P.T., Done C., Smith D.A., 1998a, ApJL, 496, 25
Życki P.T., Done C., Smith D.A., 1998b, MNRAS, submitted
Życki P.T., Czerny, B. 1994, MNRAS, 266, 653
Życki P.T., Krolik J.H., Zdziarski A.A., Kallman T.R., 1994,
ApJ., 437, 597.